(Received 10 January 2026, Accepted 29 January 2026, Scheduled 20 February 2026)

Synergistically Optimized Vivaldi Array with SSPP Decoupling and Metasurface Gain Enhancement

Shuangshuang Zhu[1], Yang Shao[1], Zeting Li[2], Xiaoyuan Wang[1], Xinlong Bi[1], Yunjie Song[1], and Zhi Quan[1,*]

[1] School of Electrical and Information Engineering, Zhengzhou University, Zhengzhou 450001, China
[2] School of Information and Communications Engineering, Xi'an Jiaotong University, Xi'an 710049, China

ABSTRACT: This study proposes a two-element Vivaldi antenna array that achieves broadband mutual coupling suppression and gain enhancement. First, by etching multiple spoof surface plasmon polariton (SSPP) slots on the ground plane to suppress surface-wave coupling, the inter-element isolation has increased from 20–31 dB to 20–45 dB, with an improvement of 5–10 dB (a peak of 20 dB) within the operating band of 1.8–4.5 GHz. Then, a quasi-transparent metasurface (MS) is placed above the aperture to enable phase compensation, converting spherical wavefronts to quasi-planar ones and thereby improving the gain of 0.5–2 dBi across the operating band. Finally, the designed Vivaldi antenna array is fabricated and measured, which exhibits $S_{11} < -10$ dB (1.3–4.5 GHz), enhanced isolation, and stable gain performance.

1. INTRODUCTION

Vivaldi antenna has been widely adopted in broadband applications owing to its wide impedance bandwidth, high gain, and stable radiation characteristics [1–3]. Its exponentially tapered slot structure enables an efficient transition from guided waves to radiated waves, making it suitable for modern electromagnetic systems such as 5G/6G communications, radar, and ultra-wideband (UWB) sensing [4–6]. However, in Vivaldi antenna array configurations, strong mutual coupling between adjacent elements is a major issue that degrades performance, causing impedance mismatch, radiation pattern distortion, and gain reduction [7–9].

Several approaches have been explored to mitigate the mutual coupling in Vivaldi antenna arrays, including defected ground structures (DGSs) [10], decoupling networks [11], and metamaterial-based isolators [12]. However, these methods often suffer from limitations, such as narrow bandwidth, added loss, and design complexity. Recently, spoof surface plasmon polariton (SSPP) structures have been used to reduce the mutual coupling in Vivaldi antenna arrays by constraining transmission wave [13]. Nevertheless, this method is not effective for lower frequency bands.

Another key challenge is achieving high gain without compromising the low-profile structure or impedance bandwidth. Traditional gain enhancement approaches, such as dielectric lenses or directors, tend to increase volume or complexity [14–16]. Metasurface-based techniques offer a promising alternative for improving directivity and aperture efficiency by manipulating the phase front [17]. However, many reported designs are limited by their narrow bandwidths and poor compatibility with decoupling structures.

To address these challenges, this paper presents a Vivaldi antenna array that integrates SSPP structures for mutual coupling reduction and metasurface (MS) for gain enhancement. The SSPP slots suppress surface waves, which is different from the previous work, while the metasurface flattens the phase front. Together, both improved isolation (with an average improvement of 5–10 dB) and enhanced gain (by 0.5–2 dBi) across 1.8–4.5 GHz can be achieved. The measurements demonstrate that the proposed Vivaldi antenna array maintains good matching, stable radiation performance, and a compact profile, making it suitable for wideband sensing and communication systems.

2. VIVALDI ANTENNA ARRAY DESIGN

The initial Vivaldi antenna array, denoted as Ant-I, is shown in Fig. 1(a). The structure comprises three layers: radiating arms are printed on the top layer; a feeding network is on the bottom layer; and a dielectric substrate of Rogers RO4350B with a thickness of 1 mm-, dielectric constant of 3.5, and loss tangent of 0.0037 lies between the layers. The feed uses a microstrip-to-slotline transition, with a tapered slot profile defined by the exponential curves:

$$y_1 = 0.5w_1 \times \exp\left(\frac{x\ln(w/w_1)}{l_x}\right) + l_d \quad (0\,\text{mm} \le x \le 80\,\text{mm}) \tag{1}$$

where $l_x = 80$ mm and $l_d = 20$ mm. Full-wave simulations by using High Frequency Structure Simulator (HFSS) were performed to understand the behavior of Ant-I. The reflection coefficient (S_{11}) of Ant-I is shown in Fig. 2(a), indicating an impedance bandwidth ($S_{11} < -10$ dB) from 1.5 GHz to beyond 4.5 GHz. The coupling coefficient (S_{21}) of Ant-I is shown in

* Corresponding author: Zhi Quan (iezquan@zzu.edu.cn).

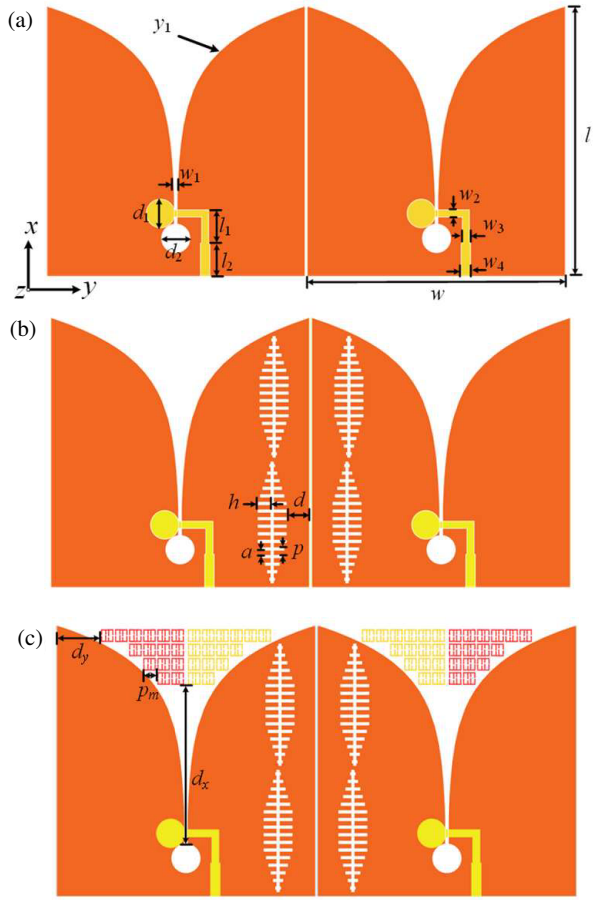

FIGURE 1. Configurations of the proposed (a) Ant-I, (b) Ant-II, and (c) Ant-III. The geometrical parameters are $l = 114$, $w = 110$, $d_1 = 6$, $d_2 = 7$, $l_1 = 9$, $l_2 = 12$, $w_1 = 1.2$, $w_2 = 1$, $w_3 = 1.5$, $w_4 = 2$, $h = 6.5$, $d = 8$, $p = 3.2$, $a = 1$, $d_x = 40.5$, $d_y = 19$, $p_m = 6$. All in millimeters.

Fig. 2(b), where the values are approximately -22 dB within the operating band.

2.1. Ant-I with SSPP

To suppress the mutual coupling observed in Ant-I, spoof surface plasmon polariton (SSPP) slot structures were etched on the ground plane between the Vivaldi antenna elements. The resulting design is denoted as Ant-II, as shown in Fig. 1(b). The dispersion curve of the SSPP unit is shown in Fig. 3, confirming its slow-wave properties and potential to suppress surface-wave coupling in the target band. The larger the h is, the lower the cutoff frequency of SSPP is, and the lower the frequency of electromagnetic waves passing through SSPP is.

After integrating the SSPP slots, Ant-II generally exhibited reduced mutual coupling compared to Ant-I, as shown in Fig. 2(b). However, a slight increase in coupling was observed around 1.7 GHz. This is attributed to the lack of efficient mode conversion at lower frequencies, which limits the confinement of the surface waves by the SSPP grooves. As a result, surface waves near 1.7 GHz can propagate toward the adjacent Vivaldi antenna element.

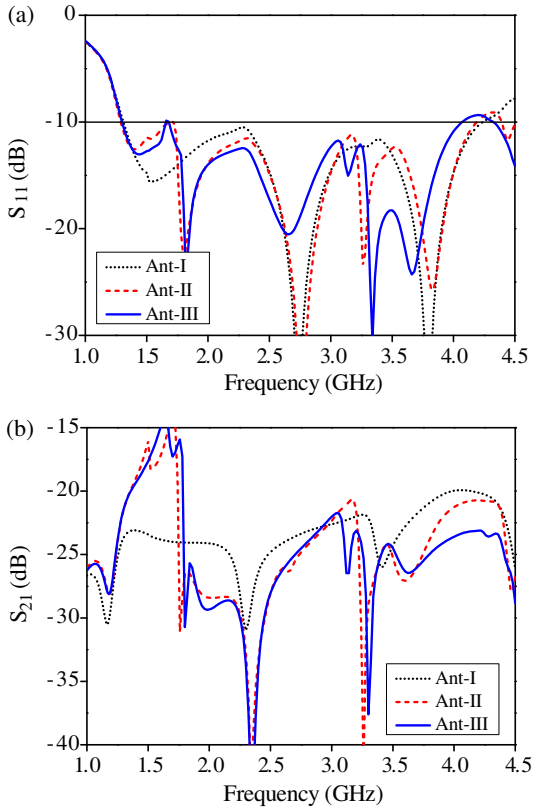

FIGURE 2. Simulated (a) S_{11} and (b) S_{21} of Ant-I, Ant-II, and Ant-III.

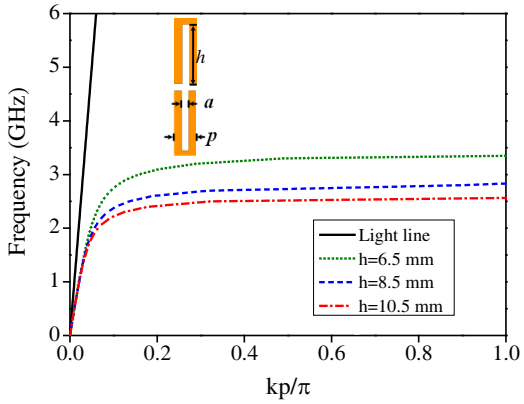

FIGURE 3. Simulated dispersion diagrams of the SSPP structure for different groove depths. $p = 3.2$ mm, and $a = 1$ mm.

To evaluate the influence of groove depth on the performance, Fig. 4 presents the transmission characteristics of the SSPP-based slot line for three groove depths ($h = 6.5$ mm, 8.5 mm, and 10.5 mm). The corresponding cutoff frequencies were approximately 3.2 GHz, 3.0 GHz, and 2.7 GHz, respectively, aligned with the dispersion trends in Fig. 3. Although frequencies below these cutoffs are nominally confined, the lack of effective mode conversion weakens the wave confinement at the lower band edge, leading to the noted increase in coupling near 1.7 GHz.

To further validate the design, Figs. 5(a) and (b) present the simulated S_{11} and S_{21} of Ant-II under the three SSPP groove depths, respectively. It is observed that at depths $h = 6.5$ mm,

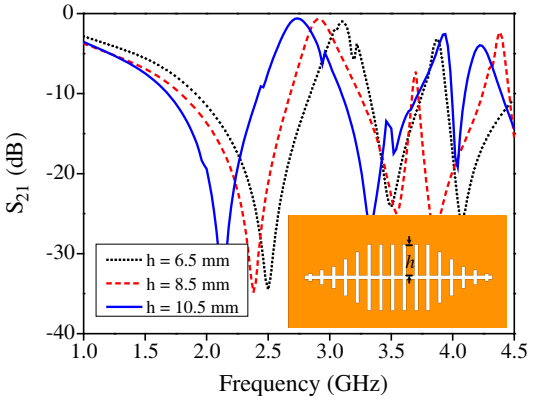

FIGURE 4. The simulated S_{21} of SSPP slot structure.

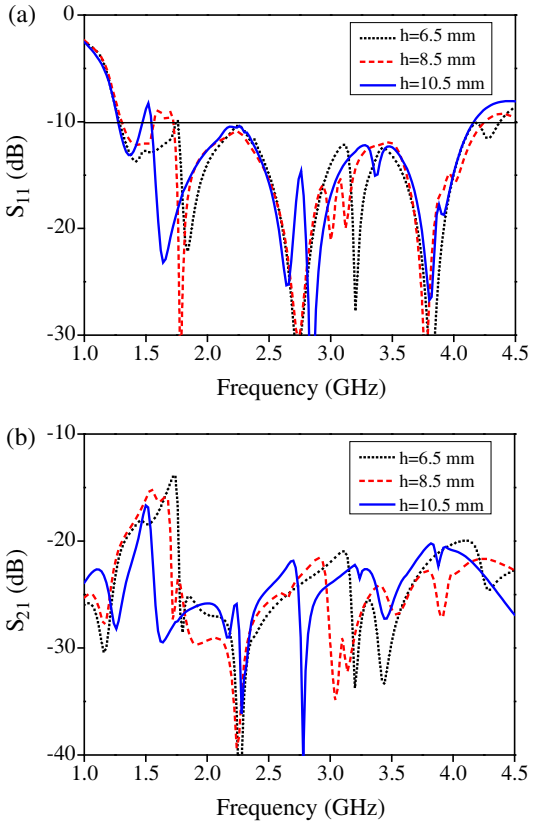

FIGURE 5. Effects of SSPP structure on (a) S_{11} and (b) S_{21} characteristics of Ant-II.

8.5 mm, and 10.5 mm, the simulated S_{21} of Ant-II increases notably around 3.2 GHz, 3.0 GHz, and 2.7 GHz, respectively — consistent with the cutoff behavior shown in Figs. 3 and 4. Based on the evaluation of both S_{11} and S_{21} across the band, the groove depth $h = 6.5$ mm was selected for Ant-II, because it maintains good matching while providing effective decoupling over the widest portion of the operating band.

2.2. Ant-II with MS

To further enhance the radiation performance without compromising the bandwidth achieved in Ant-II, a quasi-transparent MS was placed above the radiating aperture. This final configuration is denoted as Ant-III, as shown in Fig. 1(c). The MS is designed based on a phase compensation principle to reshape the wavefront, which gradually converts the original spherical wavefront into a quasi-planar wavefront, thereby improving the directivity in the end-fire direction.

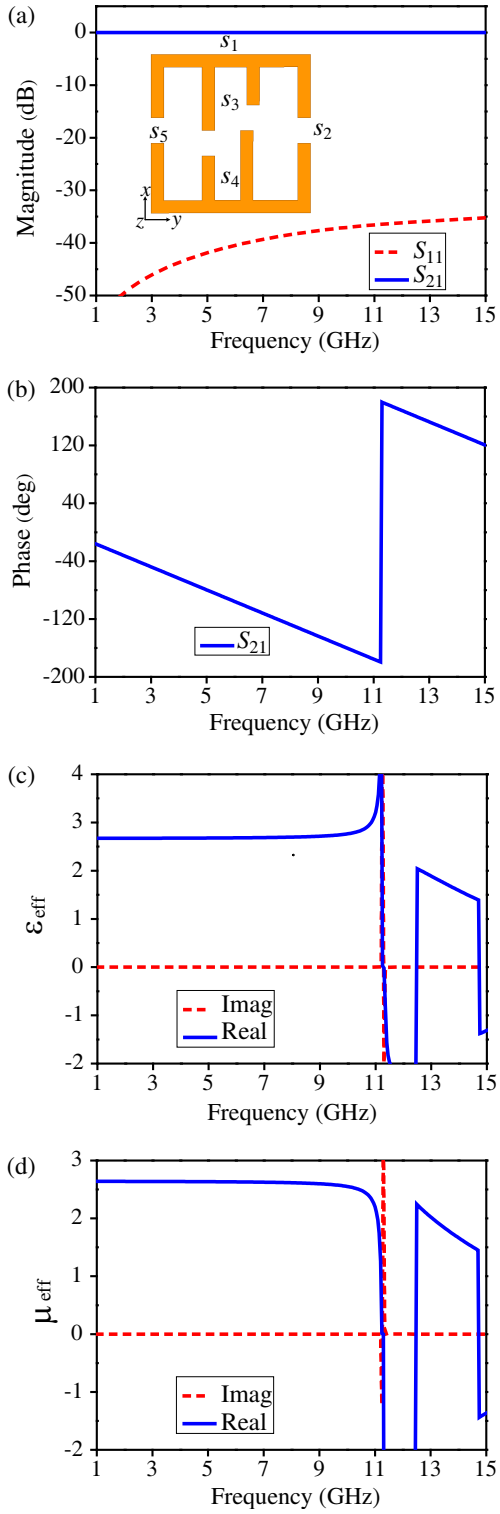

FIGURE 6. Characteristics of MS. (a) S-parameters, (b) transmission phase, (c) effective permittivity, and (d) effective permeability under y-polarization. $s_1 = 5$ mm, $s_2 = 5$ mm, $s_3 = 2.4$ mm, $s_4 = 1.6$ mm, and $s_5 = 0.2$ mm.

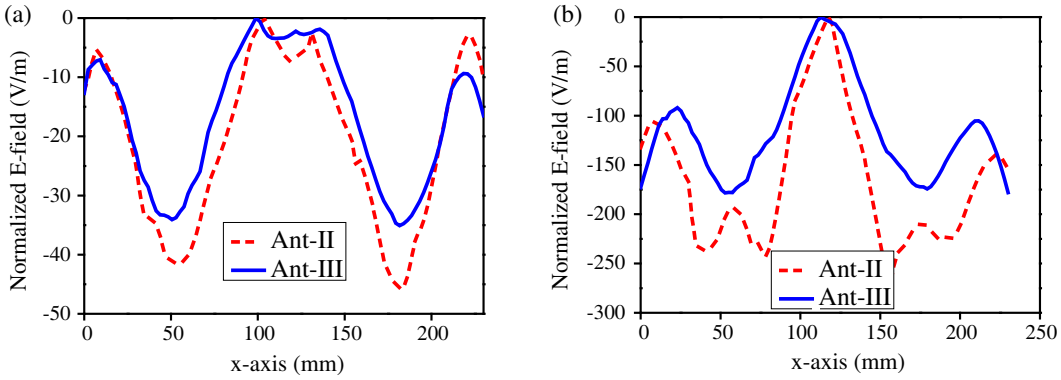

FIGURE 7. Comparison of the phase distribution along y-direction in the reference plane, with and without MS at (a) 2.5 GHz and (b) 4 GHz.

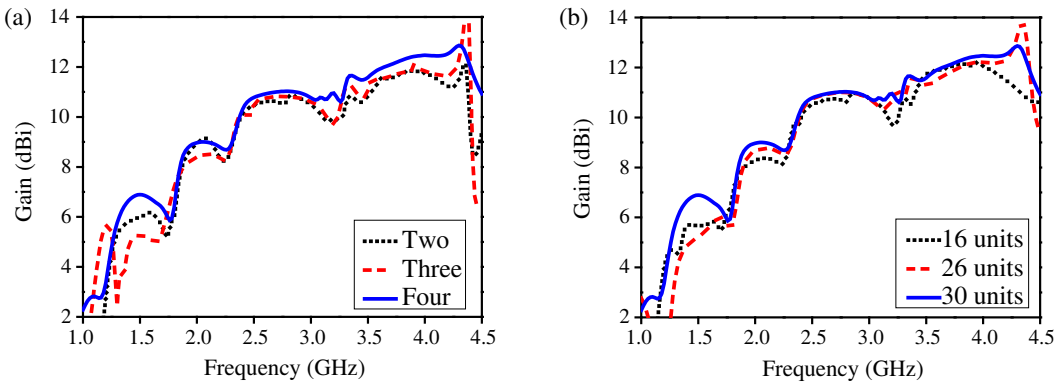

FIGURE 8. Simulated gains of Ant-III with MS of (a) different layers (count along the x-axis) and (b) different unit cells (starting from the center of the radiation slot and counting to the sides).

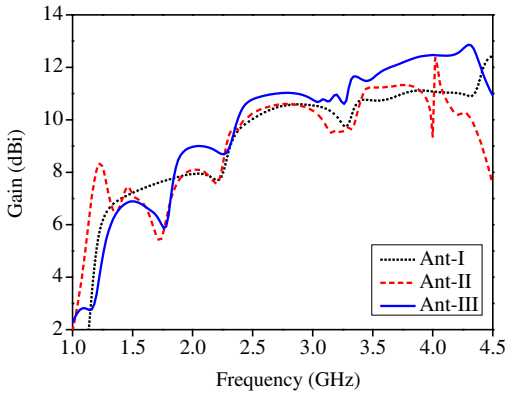

FIGURE 9. Simulated gains of Ant-I, Ant-II, and Ant-III.

Figure 6(a) shows the unit cell of the designed MS (depicted in the inset) along with the simulated transmission and reflection magnitudes. The unit achieves high transmission and low reflection across 1–15 GHz, ensuring minimal disturbance of the inherent radiation of the Vivaldi antenna. The corresponding transmission phase is plotted in Fig. 6(b), which provides the necessary phase gradient for wavefront flattening. Furthermore, Figs. 6(c) and (d) show the retrieved effective permittivity and permeability, confirming the broadband operation and compatibility with the impedance characteristics of the Vivaldi antenna.

The improvements in near-field distributions are demonstrated in Fig. 7, which compares the normalized electric-field distributions of Ant-II and Ant-III at 2.5 GHz and 4 GHz. When the MS was loaded, the field uniformity along the radiation aperture of the Vivaldi antenna array was significantly enhanced, leading to a more complanate wavefront. To evaluate the influence of the number of MS layers and unit cells on the performance, Fig. 8 presents the simulated gains of Ant-III. As can be seen, different layer numbers and unit cells have an impact on the antenna's gain. Eventually, 4 layers and 30 units were used in the design to enhance the antenna's gain.

To verify the improvement in Ant-II performance by loading the designed MS, Fig. 9 shows the simulated gains of Ant-I, Ant-II, and Ant-III. It can be seen that Ant-III exhibits a gain improvement of approximately 0.5–2 dBi over Ant-I within 1.8–4.5 GHz, validating the effectiveness of the MS in improving end-fire radiation while maintaining the decoupling benefits achieved in Ant-II.

3. MEASURED RESULTS

A prototype of Ant-III was fabricated and measured to validate the feasibility of the proposed design approach, as presented in Fig. 10. The S-parameters were measured using a Keysight N5227B vector network analyzer. Fig. 11(a) shows the measured S_{11} and S_{21} of Ant-III, which shows agreement with the simulated results across the operating band 1.3–4.5 GHz, con-

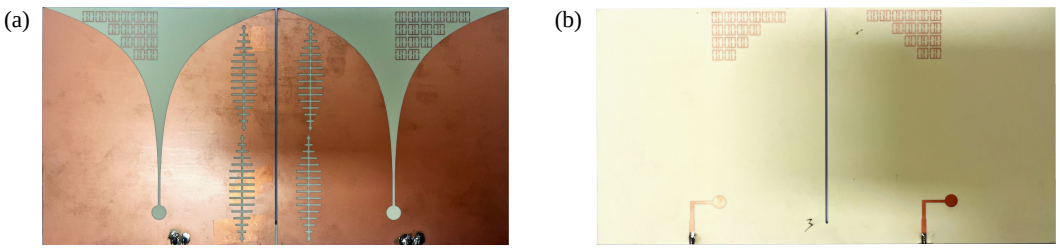

FIGURE 10. The photographs of the fabricated Ant-III, (a) top and (b) bottom.

TABLE 1. Comparison between the proposed Vivaldi antenna arrays.

Ref. No.	Number of element	Operating frequency (GHz)	Min-Max gain (dBi)	Size ($\lambda_g \times \lambda_g \times \lambda_g$)	Frequency band of mutual coupling reduction (GHz)	Isolation (dB)
[1]	2	0.6–3	NA	$0.3 \times 0.186 \times 0.121$	0.6–3	10–48
[11]	8	6–18	6–13.5	$5.29 \times 3.87 \times 0.48$	6–15	13–50
[13]	8	22–24	9.56–10.1	$5.56 \times 2.52 \times 0.073$	22–24	18–21
[18]	2	2–10	3.9–10.2	$1.34 \times 0.67 \times 0.0178$	2–10	20–35
[19]	8	7.5–12.5	6–16.5	$3.7 \times 3.33 \times 0.056$	7.5–12.5	13–28
This work	2	1.25–4.5	6–12	$1.375 \times 0.71 \times 0.0057$	1.8–4.5	22–46

λ_g is the guided wavelength at the lowest frequency of the resonant band.

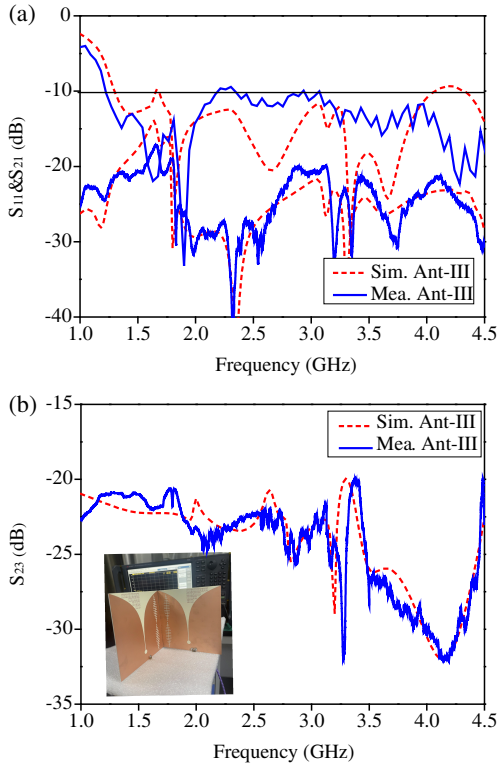

FIGURE 11. Measured and simulated results of Ant-III. (a) S_{11} and S_{21}, (b) S_{23}.

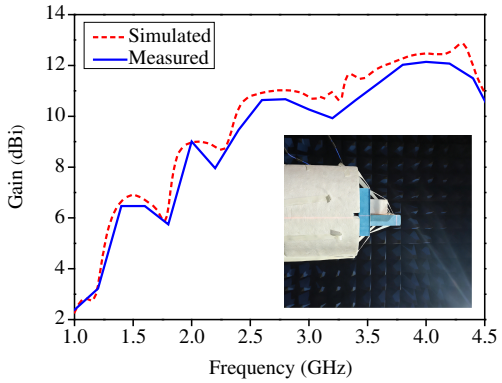

FIGURE 12. Measured and simulated gains of Ant-III.

firming accurate impedance matching. The measurement errors mainly result from processing and welding issues. Subsequently, the designed decoupling method will be applied to a 2–4 GHz dual-polarization Vivaldi antenna array. Therefore, the mutual coupling of dual-polarization Vivaldi antenna units was also measured. Fig. 11(b) shows the mutual coupling between the Vivaldi antennas at two adjacent ports. It can be seen that the polarization coupling remains below -20 dB within the working frequency band, which satisfies most high-precision systems, such as radars and 5G/6G base stations.

Radiation performance was tested in an anechoic chamber with a standard horn antenna as the reference. Fig. 12 presents a comparison between the simulated and measured gains. The simulated gain is 6–12.9 dB, and the measured gain is 6–12 dB in the operating band. The error in measured gain mainly stems from the fact that the radiation directions of the standard horn and test antenna are not perfectly aligned, which results in an error between the test gain and simulation gain. Moreover, the measured radiation patterns of Ant-III at 2 GHz, 3 GHz, and 4 GHz are given in Fig. 13, where they maintain good agreement with the simulations and show stable end-fire radiation characteristics.

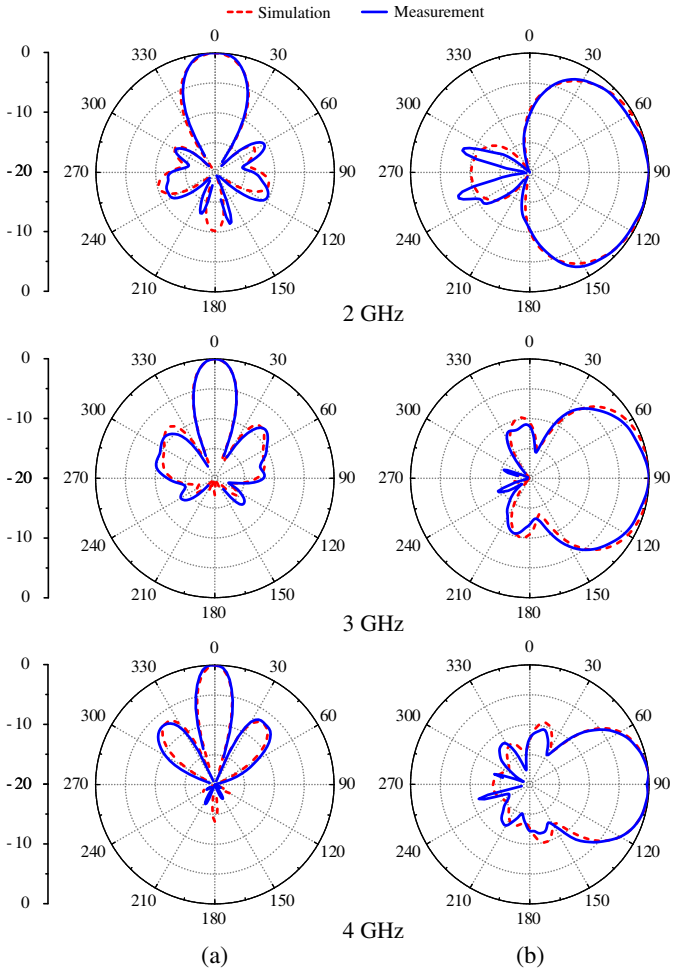

FIGURE 13. Measured and simulated radiation patterns of Ant-III at (a) xoy-plane and (b) xoz-plane.

To highlight the superiority of the designed Vivaldi antenna array, several Vivaldi antenna arrays in terms of operating band, gain, size, and mutual coupling are given in Table 1. The decoupling methodologies include metasurface-only (Ref. [11]), SSPP-only (Ref. [13]), and DGS-only (Ref. [18]). Compared with the method in [13] that reduces mutual coupling by restricting the transmission waves, this work proposes a method based on suppressing the transmission of surface waves to reduce mutual coupling. Existing designs often enhance one performance parameter at the expense of others, such as gaining wideband with limited coupling or achieving high gain with an enlarged coupling. The proposed work achieves both effective coupling reduction and gain enhancement within the required working frequency band, demonstrating a balanced advancement for wideband systems.

4. CONCLUSION

This study demonstrates a Vivaldi antenna array that integrates SSPP decoupling and an MS for gain enhancement. The combined approach effectively addresses the mutual coupling and directivity limitations within a single, low-profile structure. The fabricated prototype measurements validate concurrent improvements in isolation (22–46 dB) and realized gain (6–12 dBi) across the 1.8–4.5 GHz band, while maintaining wide impedance matching. The design offers a balanced and practical solution for wideband systems, demonstrating its potential for applications such as microwave imaging and advanced communication systems. The limitation of this design lies in the fact that the working frequency band of SSPP is related to its size. Using a conventional SSPP structure makes it difficult to achieve decoupling in the low-frequency range. The future work will continue to explore the new SSPP slot structure, thereby further expanding the decoupled frequency band to the entire frequency range. Then, the proposed decoupling method will be extended to the dual-polarization Vivaldi array to meet the requirements of MIMO systems.

ACKNOWLEDGEMENT

The authors express their thank and acknowledge to the support from the National Natural Science Foundation of China (62201509), the Youth Talent Support Program of Henan Association for Science and Technology (2025HYTP064), and the Science and Technology Research Project of Henan Province (242102210181).

REFERENCES

[1] Wang, M., L. Crocco, S. Costanzo, R. Scapaticci, and M. Cavagnaro, "A compact slot-loaded antipodal Vivaldi antenna for a microwave imaging system to monitor liver microwave thermal ablation," *IEEE Open Journal of Antennas and Propagation*, Vol. 3, 700–708, 2022.

[2] Guo, Y., T. Deng, J. Xu, X. Huang, and X. Wei, "A wideband phased array RF front end with coupling-capture channels for full-duplex wireless backhaul," *IEEE Transactions on Microwave Theory and Techniques*, Vol. 73, No. 10, 8258–8274, Oct. 2025.

[3] Zhang, Y., P.-F. Gu, Z. He, H.-G. Bao, J. Xu, J.-X. Sun, Y.-J. Cheng, Z.-H. Fan, and D.-Z. Ding, "An irregular optimizing design of connected Vivaldi array for wideband and wide-angle scanning," *IEEE Transactions on Antennas and Propagation*, Vol. 73, No. 6, 3743–3756, Jun. 2025.

[4] Cheng, H., S. Li, Y. Fu, H. Yang, J. Wu, X. Zhou, and X. Shi, "Integration of SSPP antenna and Vivaldi arrays for 5G sub-6 GHz and millimeter-wave applications," *IEEE Antennas and Wireless Propagation Letters*, Vol. 24, No. 7, 2099–2103, Jul. 2025.

[5] Bergman, J. H. S., M. Heino, J. Ala-Laurinaho, T. Riihonen, M. Valkama, and V. Viikari, "Design of aperture-coupled Vivaldi-antenna array with scan-range-improving parasitic resonators for Ka-band," *IEEE Transactions on Antennas and Propagation*, Vol. 73, No. 9, 6955–6960, Sep. 2025.

[6] Li, J., H. Zhai, and M. Wang, "A compact Vivaldi antenna with enhanced bandwidth and mismatch suppression," *IEEE Transactions on Antennas and Propagation*, Vol. 73, No. 1, 623–628, Jan. 2025.

[7] Ge, F., H. Zhao, M. Yang, S. Li, and X. Yin, "Ku-band small frequency ratio self-diplexing Vivaldi antenna with high isolation for high-power application," *IEEE Antennas and Wireless Propagation Letters*, Vol. 24, No. 8, 2682–2686, Aug. 2025.

[8] Craeye, C. and D. González-Ovejero, "A review on array mutual coupling analysis," *Radio Science*, Vol. 46, No. 2, 1–25, Apr. 2011.

[9] Zou, X.-J., Y.-W. Wang, B.-F. Zong, X.-G. Xu, L.-X. Han, H. Zhu, W. Song, M. Tan, and H.-N. Du, "Miniaturized low-profile ultrawideband antipodal Vivaldi antenna array loaded with edge techniques," *IEEE Transactions on Antennas and Propagation*, Vol. 74, No. 1, 1156–1161, 2026.

[10] Zhu, S., H. Liu, Z. Chen, and P. Wen, "A compact gain-enhanced Vivaldi antenna array with suppressed mutual coupling for 5G mmWave application," *IEEE Antennas and Wireless Propagation Letters*, Vol. 17, No. 5, 776–779, May 2018.

[11] Li, J. and H. Zhai, "A wideband grating lobe suppression scheme based on array factor reconfiguration and its application in multi-beam antenna arrays," *IEEE Transactions on Antennas and Propagation*, Vol. 73, No. 11, 8601–8611, Nov. 2025.

[12] Gupta, S., Z. Briqech, A. R. Sebak, and T. A. Denidni, "Mutual-coupling reduction using metasurface corrugations for 28 GHz MIMO applications," *IEEE Antennas and Wireless Propagation Letters*, Vol. 16, 2763–2766, Oct. 2017.

[13] Zhu, S., H. Liu, and Z. Chen, "An antipodal Vivaldi antenna array based on spoof surface plasmon polariton metamaterial with 5G mm Wave suppression," *Journal of Physics D: Applied Physics*, Vol. 54, No. 28, 28LT02, May 2021.

[14] Huang, W., Y. Xiao, G. Zhao, J. Hu, and Z. Chen, "Ultra-wideband tapered slot antenna with phasecorrecting dielectric lens loaded," *IEEE Antennas and Wireless Propagation Letters*, Vol. 23, No. 12, 4218–4222, Dec. 2024.

[15] Zhao, G., Y. Xiao, W. Huang, S. Xu, and Z. Chen, "Compact and gain-enhanced Vivaldi antenna design using nonuniform slot profile optimization and aperture dielectric loading," *IEEE Antennas and Wireless Propagation Letters*, Vol. 24, No. 7, 1570–1574, Jul. 2025.

[16] Kim, I., H.-Y. Lee, D.-M. Lee, H.-J. Lee, H. Kim, E.-S. Kim, and N.-Y. Kim, "Broadband gain enhanced narrow-beam Vivaldi antenna with ring and directors for handheld antidrone jamming system," *IEEE Antennas and Wireless Propagation Letters*, Vol. 23, No. 1, 214–218, Jan. 2024.

[17] Shi, X., Y. Cao, Y. Hu, X. Luo, H. Yang, and L. H. Ye, "A high-gain antipodal Vivaldi antenna with director and metamaterial at 1–28 GHz," *IEEE Antennas and Wireless Propagation Letters*, Vol. 20, No. 12, 2432–2436, Dec. 2021.

[18] Nurhayati, , G. Hendrantoro, T. Fukusako, and E. Setijadi, "Mutual coupling reduction for a UWB coplanar Vivaldi array by a truncated and corrugated slot," *IEEE Antennas and Wireless Propagation Letters*, Vol. 17, No. 12, 2284–2288, Dec. 2018.

[19] Kazemi, R., A. E. Fathy, and R. A. Sadeghzadeh, "Dielectric rod antenna array with substrate integrated waveguide planar feed network for wideband applications," *IEEE Transactions on Antennas and Propagation*, Vol. 60, No. 3, 1312–1319, Mar. 2012.